remote sensing

MDPI

Technical Note

The Extended H_∞ Particle Filter for Attitude Estimation Applied to Remote Sensing Satellite CBERS-4

William Reis Silva [1,*], Roberta Veloso Garcia [2], Paula C. P. M. Pardal [3], Hélio Koiti Kuga [4], Maria Cecília F. P. S. Zanardi [5] and Leandro Baroni [6]

1 Gama Campus (FGA), University of Brasilia (UnB), Área Especial de Indústria, Projeção A, Setor Leste (Gama), Brasília 72444-240, DF, Brazil
2 Lorena School of Engineering (EEL), University of São Paulo (USP), Estrada Municipal do Campinho, S/N. Ponte Nova, Lorena 12602-810, SP, Brazil
3 Collaborative Laboratory (CoLAB), Center of Engineering and Product Development (CEiiA), PACT, Rua Luís Adelino Fonseca, 1, 7005-841 Évora, Portugal
4 Space Mechanics and Control Division (DMC), National Institute for Space Research (INPE), Av. dos Astronautas, 1758, Jardim da Granja, São José dos Campos 12227-010, SP, Brazil
5 Campus Guaratinguetá (FEG), São Paulo State University (UNESP), Av. Dr. Ariberto Pereira da Cunha, 333, Pedregulho, Guaratinguetá 12516-410, SP, Brazil
6 Engineering, Modeling and Applied Social Sciences Center (CECS), Federal University of ABC (UFABC), Av. dos Estados, 5001, Bangú, Santo André 09210-580, SP, Brazil
* Correspondence: reis.william@unb.br; Tel.: +55-61-99632-0060

Abstract: An extension of the linear H_∞ filter, presented here as the extended H_∞ particle filter (EH_∞PF), is used in this work for attitude estimation, which presents a process and measurement model with nonlinear functions. The simulations implemented use orbit and attitude data from CBERS-4 (China–Brazil Earth Resources Satellite-4), making use of the robustness characteristics of the H_∞ filter. The CBERS-4 is the fifth satellite of an advantageous international scientific interaction between Brazil and China for the development of remote sensing satellites used for strategic application in monitoring water resources and controlling deforestation in the Legal Amazon. In the extended H_∞ particle filter (EH_∞PF) the nature of the system, composed of dynamics and noises, seeks to degrade the state estimate. The EH_∞PF deals with this by aiming for robustness, using a performance parameter in its cost function, in addition to presenting an advantageous feature of using a reduced number of particles for state estimation. The justification for the application of this method is because the non-Gaussian uncertainties that appear in the attitude sensors impair the estimation process and the EH_∞PF minimizes in signal estimation the worst effects of disturbance signals without a priori knowledge of them, as shown in the results, in addition to presenting good precision within the prescribed requirements, with 100 particles representing a processing time 2.09 times less than the PF with 500 particles.

Keywords: extended H_∞ particle filter; particle filter; nonlinear state estimation; attitude estimation; China–Brazil Earth Resources Satellite

Citation: Silva, W.R.; Garcia, R.V.; Pardal, P.C.P.M.; Kuga, H.K.; Zanardi, M.C.F.P.S.; Baroni, L. The Extended H_∞ Particle Filter for Attitude Estimation Applied to Remote Sensing Satellite CBERS-4. *Remote Sens.* **2023**, *15*, 4052. https://doi.org/10.3390/rs15164052

Academic Editor: Jianguo Yan

Received: 26 June 2023
Revised: 28 July 2023
Accepted: 14 August 2023
Published: 16 August 2023

1. Introduction

Remote sensing satellite missions require pointing, so an accurate attitude determination and control system is a dominant factor for mission success. The attitude sensor determines how a given reference vector is oriented in relation to the satellite system [1]. After processing these vectors computationally, it is then possible to estimate the satellite's orientation using attitude estimation techniques. With the advancement in technologies, the computational power and energy efficiency of microprocessors enables the use of increasingly computationally heavy models [2]. This strategy is especially advantageous in space systems.

The main objective of this research is to analyze the feasibility along with the advantages and disadvantages of implementing the EH_∞PF for attitude estimation, highlighting and expanding the properties of the H_∞ filter, showing its advantageous characteristics. In the EH_∞PF the nature of the system, composed of dynamics and noises, seeks to deteriorate the state estimate, while at the same time seeking robustness through a coefficient of performance in its respective cost function. These characteristics of the method provide, with a reduced number of particles, a good processing time and good precision without sample impoverishment.

The justification for this research is given by the fact that many spacecraft missions, not only the remote sensing ones such as the CBERS-4 used in this research, necessitate precise sensor pointing and precise determination and attitude control in real time, which entails estimating attitude and gyros bias from attitude measurements provided by sensor outputs. The correct attitude determination directly influences the performance of the attitude control system and adjacent systems on the satellite that need this information. According to [3], because the determination of attitude is done using sensors, whose measurements always include some noise and non-Gaussian uncertainties, stochastic filters are more suitable approaches. The non-Gaussian uncertainties that appear in the process model are contained in the gyro's measurements, which present noise and bias due to post-launch sensor misalignment, thermal expansion, fading, electro-mechanical degradation, etc. All these factors cause inaccuracies in the model and deteriorate the attitude estimation process. Thus, the EH_∞PF deals well with this problem as shown in the results of this research.

The EH_∞PF algorithm uses the H_∞ robust filter concept so that external interference is overcome [4]. The H_∞ filtering minimizes the worst-case estimation error using the concepts from the famous game theory approach [5–7]. The second-order linearization for the H_∞ filtering was presented more recently in [8]. For the H_∞ robust filtering, the parameter γ has a special meaning for the method; it evaluates the upper threshold level and verifies the robustness of the H_∞ robust filtering for the uncertain interference [3,4]. The performance is associated with the appropriate choice of the γ parameter, which is directly associated with robustness and the average accuracy of the system [9], where you should always try to find a balance between these method properties. The finding is that with a higher the value of γ, the result will be closer to a normal filtering. The lower the associated γ value, the more intense the filter robustness [4,10].

The CBERS-4 attitude and gyros bias estimation, which makes use of the PROPAT propagator [11], analyzing and comparing the mean error, standard deviation, root mean squared error (RMSE), and the processing time cost of the estimation methods used is the main aim of this research. The simulations are implemented with orbit and attitude data from 1 September 2015 provided by the Satellite Control Center of the Brazilian National Institute for Space Research (CCS-INPE). The quaternions are used to represent attitude [12], and two estimation methods are used and compared—PF and EH_∞PF—which are modern methods that consider both the process model and the noisy measurement model. The application of these methods in real missions characterizes the main contribution of this work regarding the state-of-the-art estimation methods.

In aerospace engineering, it is possible to note important contributions related to the application of estimation methods: Ref. [12] presents a study on the satellite attitude estimation using the EKF; ref. [13] presents comparisons between two Kalman filters for nonlinear systems; ref. [14] analyses the results of the EKF in an instant mapping and localization process; ref. [15] research uses the EKF for attitude and gyros bias estimation but with real data and with a sampling time less than that the one used in this research; refs. [16,17] present a spacecraft attitude estimation through UKF, using quaternions and Euler angles; ref. [18] analyzes the UKF robustness for orbit determination through global positioning system signals; ref. [19] presents the orbit determination using nonlinear PF and GPS measurements; ref. [1] makes a comparison between the estimation methods of UKF, regularized particle filter (RegPF), and extended H_∞ filter (EH_∞F); and ref. [20]

presents the Rao-Blackwellized particle filter (RaoBPF) attitude estimation and gyros bias for the CBERS 4 satellite, evaluating computational processing time cost and precision.

The structure of the article is as follows: Section 2 introduces the problem statement for nonlinear state estimation. Section 3 presents the general concepts of an extended H_∞ particle filter (EH_∞PF). Section 4 presents methods applied to gyros bias estimation and attitude estimation using the CBERS-4 orbit and attitude simulation data. The results are presented, analyzing the precision of the methods and the processing time of each one. Section 5 presents some conclusions and final comments.

2. Problem Statement

Assume the process model and the measurement model that represent a system of nonlinear equations described by:

$$\begin{aligned} \boldsymbol{x}_{k+1} &= f_k(\boldsymbol{x}_k, \boldsymbol{u}_k, \boldsymbol{w}_k) \\ \boldsymbol{y}_k &= h_k(\boldsymbol{x}_k, \boldsymbol{v}_k) \end{aligned} \tag{1}$$

where the term k is the time index, $\boldsymbol{x}_k$ is the state vector, $\boldsymbol{u}_k$ is associated with the control input, $\boldsymbol{w}_k$ is the process noise, $\boldsymbol{y}_k$ is the measurement vector, and $\boldsymbol{v}_k$ is the measurement noise. The function $f_k(.)$ is commonly referred to as process equation, and $h_k(.)$ is commonly referred to as measurement equation; both functions are time-varying nonlinear vector systems. Both noises $\boldsymbol{w}_k$ and $\boldsymbol{v}_k$ are often considered Gaussian white noise and independently presented as a well-defined probability density function.

For applications of estimation methods, the process and measurement model may change from that presented by Equation (1), in which sometimes the process model is linear and the measurement model is nonlinear, or vice-versa. This happens for attitude estimation depending on the chosen parameterization. In this work, the attitude kinematic equation parameterized in quaternions will be used as a process model, which is a linear system, and the measurement model chosen is a nonlinear system.

2.1. Attitude Representation by Quaternions

The state vector is presented with the attitude representation parameterized in quaternion $\boldsymbol{q}$ and the gyro bias $\boldsymbol{\varepsilon}$ represented by [21,22]:

$$\boldsymbol{x} = \begin{bmatrix} \boldsymbol{q} & \boldsymbol{\varepsilon} \end{bmatrix}^T = \begin{bmatrix} q_1 & q_2 & q_3 & q_4 & \varepsilon_x & \varepsilon_y & \varepsilon_z \end{bmatrix}^T \tag{2}$$

According to [23], the bias is an output component that has characteristics of both deterministic and stochastic behavior that is not tied to the input the sensor is connected to.

Then, the linear system that represents the process equation of the problem is given by [12,21]:

$$\begin{bmatrix} \dot{\boldsymbol{q}} \\ \dot{\boldsymbol{\varepsilon}} \end{bmatrix} = \begin{bmatrix} \frac{1}{2}\boldsymbol{\Omega}_\omega & 0_{3\times 3} \\ 0_{3\times 4} & 0_{3\times 3} \end{bmatrix} \begin{bmatrix} \boldsymbol{q} \\ \boldsymbol{\varepsilon} \end{bmatrix} + \boldsymbol{w} \tag{3}$$

where $\boldsymbol{\omega} = \begin{bmatrix} \omega_x & \omega_y & \omega_z \end{bmatrix}^T$ is the angular velocity vector in the body frame, and $\boldsymbol{\Omega}_\omega$ is an anti-symmetric matrix formed with the components of angular velocity and has dimension 4×4, given by [12,21]:

$$\boldsymbol{\Omega}_\omega = \begin{bmatrix} 0 & \omega_z & -\omega_y & \omega_x \\ -\omega_z & 0 & \omega_x & \omega_y \\ \omega_y & -\omega_x & 0 & \omega_z \\ -\omega_x & -\omega_y & -\omega_z & 0 \end{bmatrix} \tag{4}$$

In this work, the gyros model (rate integration gyros–RIGs) was used that has the classic representation [21,22] given by $\boldsymbol{\omega}_i = \boldsymbol{g}_i - \boldsymbol{\varepsilon}_i + \boldsymbol{v}_i$, where $(i = x, y, z)$, the term $\boldsymbol{g}_i(t)$ is the gyro output vector, $\boldsymbol{\varepsilon}_i(t)$ are the components of the gyros bias defined as an output

component unrelated to the input to which the sensor is subjected, and $\boldsymbol{v}_i$ is the white Gaussian noise process, which covers all remaining non-modeled effects other than the random noises.

2.2. Mathematical Models of Attitude Sensors

The nonlinear system that represents the measurement equation of the problem is given by [24]:

$$\boldsymbol{y}_k = \begin{bmatrix} \arctan\left(\dfrac{-S_y}{S_x \cos 60^\circ + S_z \cos 150^\circ}\right) \\ 24^\circ + \arctan\left(\dfrac{S_x}{S_z}\right) \\ \phi \\ \theta \end{bmatrix} + \boldsymbol{v}_k \tag{5}$$

The first and second rows of the column matrix of Equation (5) contain the information provided by the digital sun sensor (DSS). This sensor provides the coupled *pitch* angle (α_θ, first line term) and the coupled *yaw* angle (α_ψ, second line term); the direct measurement of an attitude angle is not trackable [16,17,24]. The terms S_x, S_y, S_z are the solar vector components in the body frame, and these sensors are Chinese, made where this angle argument is associated with the field of view and resolution data sheet.

The third and fourth rows of the column matrix of Equation (5) are the information provided by the horizon sensor, commonly referred to as infrared earth sensors (IRES) [24]. Here, the roll angle measurement is given by ϕ and the pitch angle measurement is given by θ.

More information about the process and measurements equations can be found in [20].

3. The Extended H_∞ Particle Filter

The theoretical foundation of an H_∞ filter is based on a robust filter implementation [3,4] with the central goal of estimating the linear combination of the state $\boldsymbol{z}_k$, which is given by

$$\boldsymbol{z}_k = \boldsymbol{L}_k \boldsymbol{x}_k \tag{6}$$

where $\boldsymbol{L}_k$ is a full rank positive definite matrix. Commonly, $\boldsymbol{L}_k = \boldsymbol{I}$ is used to perform a direct estimate of the state $\boldsymbol{x}_k$, as in the Kalman filter. The state $\boldsymbol{z}_k$, when estimated, is represented with the notation $\hat{\boldsymbol{z}}_k$; and the initial state $\boldsymbol{x}_0$, when estimated, is represented with the notation $\hat{\boldsymbol{x}}_0$.

The central idea for the design criterion in EH_∞PF is to find $\hat{\boldsymbol{z}}_k$ that minimizes $(\boldsymbol{z}_k - \hat{\boldsymbol{z}}_k)$ for any $\boldsymbol{w}_k$, $\boldsymbol{v}_k$, and $\boldsymbol{x}_0$. The underlying concept brings the idea of a worst-case scenario; in other words, it is assumed that the nature of the system acts adversely in this estimation method, so it is necessary to find $\boldsymbol{w}_k$, $\boldsymbol{v}_k$, and $\boldsymbol{x}_0$ to maximize $(\boldsymbol{z}_k - \hat{\boldsymbol{z}}_k)$ [3,8]. This extremization problem commonly uses a cost function, where it is more convenient to put the terms $\boldsymbol{w}_k$, $\boldsymbol{v}_k$, and $\boldsymbol{x}_0$ in the denominator, represented by [3]:

$$J_1 = \frac{\sum_{k=0}^{\mathcal{N}-1} \|z_k - \hat{z}_k\|^2_{\boldsymbol{S}_k}}{\|\boldsymbol{x}_0 - \hat{\boldsymbol{x}}_0\|^2_{\boldsymbol{P}_0^{-1}} + \sum_{k=0}^{\mathcal{N}-1} \left(\|\boldsymbol{w}_k\|^2_{\boldsymbol{Q}_k^{-1}} + \|\boldsymbol{v}_k\|^2_{\boldsymbol{R}_k^{-1}} \right)} \tag{7}$$

where $\mathcal{N}$ is the number associated with the filtering range, and $k = 1, 2, ..., \mathcal{N}$. The notation $\|\boldsymbol{x}_k\|^2_{\boldsymbol{S}_k}$ is the standard representation of the weighted L_2 norm of $\boldsymbol{x}_k$, i.e., $\|\boldsymbol{x}_k\|^2_{\boldsymbol{S}_k} = \boldsymbol{x}_k^T \boldsymbol{S}_k \boldsymbol{x}_k$. The expressions $\boldsymbol{P}_0$, $\boldsymbol{Q}_k$, $\boldsymbol{R}_k$, and $\boldsymbol{S}_k$ are the weighting matrices and, by definition, are symmetric positive matrices associated with the respective problem.

For the robust filter, the direct minimization of J_1 in Equation (7) is not commonly done; the strategy is to use a performance limit redefining the cost function of the problem to find an estimate $\hat{\boldsymbol{z}}_k$, which results in [1,3]

$$J_1 < \frac{1}{\gamma} \tag{8}$$

where $\gamma \geq 0$ is the performance bound. Thus, rearranging the Equation (7) with this limiting factor results in

$$\begin{aligned} J &= -\frac{1}{\gamma}\|\boldsymbol{x}_0 - \hat{\boldsymbol{x}}_0\|^2_{\boldsymbol{P}_0^{-1}} \\ &+ \sum_{k=0}^{\mathcal{N}-1}\left[\|\boldsymbol{z}_k - \hat{\boldsymbol{z}}_k\|^2_{\boldsymbol{S}_k} - \frac{1}{\gamma}\left(\|\boldsymbol{w}_k\|^2_{\boldsymbol{Q}_k^{-1}} + \|\boldsymbol{v}_k\|^2_{\boldsymbol{R}_k^{-1}}\right)\right] < 1 \end{aligned} \tag{9}$$

The min max problem is given by the representation:

$$J^* = \min_{\hat{\boldsymbol{z}}_k} \max_{\boldsymbol{w}_k, \boldsymbol{v}_k, \boldsymbol{x}_0} J \tag{10}$$

since $\boldsymbol{v}_k = \boldsymbol{y}_k - h(\boldsymbol{x}_k)$, $\boldsymbol{z}_k = \boldsymbol{L}_k\boldsymbol{x}_k$, $\hat{\boldsymbol{z}}_k = \boldsymbol{L}_k\hat{\boldsymbol{x}}_k$ and defining $\bar{\boldsymbol{S}}_k = \boldsymbol{L}_k^T\boldsymbol{S}_k\boldsymbol{L}_k$. Thus, Equations (9) and (10) can be rewritten as

$$J^* = \min_{\hat{\boldsymbol{x}}_k} \max_{\boldsymbol{w}_k, \boldsymbol{y}_k, \boldsymbol{x}_0} J \tag{11}$$

where

$$\begin{aligned} J &= -\frac{1}{\gamma}\|\boldsymbol{x}_0 - \hat{\boldsymbol{x}}_0\|^2_{\boldsymbol{P}_0^{-1}} \\ &+ \sum_{k=0}^{\mathcal{N}-1}\left[\|\boldsymbol{x}_k - \hat{\boldsymbol{x}}_k\|^2_{\bar{\boldsymbol{S}}_k} - \frac{1}{\gamma}\left(\|\boldsymbol{w}_k\|^2_{\boldsymbol{Q}_k^{-1}} + \|\boldsymbol{y}_k - h(\boldsymbol{x}_k)\|^2_{\boldsymbol{R}_k^{-1}}\right)\right] \end{aligned} \tag{12}$$

According to [25], an optimal H_∞ filter is to find an estimate $\boldsymbol{x}_k$ that minimizes J, under the condition $\hat{\boldsymbol{x}}_0 = \arg\min\|J\|_\infty$. Since the analytical solution is by no means trivial, a suboptimal iterative algorithm is usually used to solve the optimal filter problem H_∞. In this way, we define a borderline value of performance coefficient γ, which meets $\|J\|_\infty = \sup J \leq \gamma^2$ since $\|J\|_\infty$ is the infinity-norm of J and sup is the supremum of a set [26].

3.1. Sample

Assuming a system composed of a process model and measurement model, both of which are nonlinear as shown in Equation (1), the method starts by randomly generating a considerable number N of state vectors, called particles or sample states, which will be associated with the initial probability density function (pdf) represented by $p(\boldsymbol{x}_0|\boldsymbol{Y}_0) = p(\boldsymbol{x}_0)$ [3,27]. These particles or sample states are represented as $\boldsymbol{x}_0^{+(i)}$ $(i = 1, 2, ..., N)$. This start is similar to a PF.

$$\boldsymbol{x}_0^{+(i)} \sim p(\boldsymbol{x}_0^{(i)}) \qquad (i = 1, 2, ..., N) \tag{13}$$

3.2. Prediction Step

The particles must be propagated at every step $k = 1, 2, ..., \mathcal{N}$, which must be done using the process dynamics equation $f(.)$.

$$\boldsymbol{x}_k^{-(i)} = f_{k-1}(\boldsymbol{x}_{k-1}^{+(i)}, \boldsymbol{w}_{k-1}^{(i)}) \qquad (i = 1, 2, ..., N) \tag{14}$$

where the $\boldsymbol{w}_{k-1}^{(i)}$ is called a noise vector, which is randomly generated using the well known pdf of $\boldsymbol{w}_{k-1}$ as seed.

3.3. Update Step

Once all measurements are obtained in time k, the conditional relative probabilities, also known as likelihood, of each particle $\boldsymbol{x}_k^{-(i)}$ must be calculated by pdf $p(\boldsymbol{y}_k|\boldsymbol{x}_k^{-(i)})$, which is obtained intrinsically by contributing the measurement model $h(.)$ and the noise measurements $\boldsymbol{v}_k$, represented by [3,19,20,27].

$$\begin{aligned} \delta_k^{(i)} &= p(\boldsymbol{y}_k|\boldsymbol{x}_k^{-(i)}) \\ \delta_k^{(i)} &\sim \delta_{k-1}^{(i)} \frac{1}{det\left(2\pi \boldsymbol{E}_k^{-(i)}\right)^{1/2}} exp\left(\frac{-\left|\left|\tilde{\boldsymbol{y}}_k^{(i)}\right|\right|^2_{\left(\boldsymbol{E}_k^{-(i)}\right)^{-1}}}{2} \right) \end{aligned} \tag{15}$$

where $\tilde{\boldsymbol{y}}_k^{(i)} = \boldsymbol{y}_k - \boldsymbol{H}_k^{(i)}\boldsymbol{x}_k^{-(i)}$ is the measurement residues, and the term that weights the residues $\boldsymbol{E}_k^{-(i)} = \boldsymbol{H}_k^{(i)}\boldsymbol{P}_k^{-(i)}\left(\boldsymbol{H}_k^{(i)}\right)^T + \boldsymbol{R}_k$ is the associated covariance matrix.

As a standard procedure, one should always normalize likelihood obtained by Equation (15) as follows:

$$\tilde{\delta}_k^{(i)} = \frac{\delta_k^{(i)}}{\sum_{j=1}^{N} \delta_k^{(j)}}, \tag{16}$$

in which it will be guaranteed that the sum of all likelihoods will be unitary.

The update of the covariance matrix and the state vector in this method is done using the extended H_∞ filter measurement update equations presented below.

$$\bar{\boldsymbol{S}}_k^{(i)} = \left(\boldsymbol{L}_k^{(i)}\right)^T \boldsymbol{S}_k^{(i)} \boldsymbol{L}_k^{(i)} \tag{17}$$

$$\boldsymbol{K}_k^{(i)} = \boldsymbol{P}_k^{-(i)}\left(\boldsymbol{I} - \gamma\bar{\boldsymbol{S}}_k^{(i)}\boldsymbol{P}_k^{-(i)} + \left(\boldsymbol{H}_k^{(i)}\right)^T \boldsymbol{R}_k^{-1}\boldsymbol{H}_k^{(i)}\boldsymbol{P}_k^{(i)}\right)^{-1}\left(\boldsymbol{H}_k^{(i)}\right)^T \boldsymbol{R}_k^{-1} \tag{18}$$

$$\boldsymbol{x}_k^{+(i)} = f(\boldsymbol{x}_k^{-(i)}, \boldsymbol{\mu}_k) + \boldsymbol{F}_k^{(i)}\boldsymbol{K}_k^{(i)}\left(\boldsymbol{y}_k - h\left(\boldsymbol{x}_k^{-(i)}\right)\right) \tag{19}$$

$$\boldsymbol{P}_k^{+(i)} = \boldsymbol{F}_k^{(i)}\boldsymbol{P}_k^{-(i)}\left(\boldsymbol{I} - \gamma\bar{\boldsymbol{S}}_k^{(i)}\boldsymbol{P}_k^{-(i)} + \left(\boldsymbol{H}_k^{(i)}\right)^T \boldsymbol{R}_k^{-1}\boldsymbol{H}_k^{(i)}\boldsymbol{P}_k^{(i)}\right)^{-1}\left(\boldsymbol{F}_k^{(i)}\right)^T + \boldsymbol{Q}_k \tag{20}$$

where $\boldsymbol{L}_k^{(i)}$ and $\boldsymbol{S}_k^{(i)}$ are positive matrices defined with full rank; the process and measurement Jacobians are represented by $\boldsymbol{F}_k^{(i)} = \frac{df}{d\boldsymbol{x}_k}\Big|_{\boldsymbol{x}_k=\boldsymbol{x}_k^{-(i)}}$ and $\boldsymbol{H}_k^{(i)} = \frac{dh}{d\boldsymbol{x}_k}\Big|_{\boldsymbol{x}_k=\boldsymbol{x}_k^{-(i)}}$; the performance coefficient γ has a borderline value that must satisfy the Riccati inequality represented by Equation (21), i.e., the optimized value of $\hat{\boldsymbol{x}}_k$ will be guaranteed to be a local minimum of the problem's cost function [3,8,25]:

$$\left(\boldsymbol{P}_k^{-(i)}\right)^{-1} - \gamma\bar{\boldsymbol{S}}_k^{(i)} + \left(\boldsymbol{H}_k^{(i)}\right)^T \boldsymbol{R}_k^{-1}\boldsymbol{H}_k^{(i)} > 0 \tag{21}$$

where Equation (21) must be positive definite.

Finally, the optimal state estimate and the associated error covariance matrix are calculated as:

$$\hat{\boldsymbol{x}}_k = \sum_{i=1}^{N} \tilde{\delta}_k^{(i)}\, \boldsymbol{x}_k^{+(i)} \tag{22}$$

$$\hat{\boldsymbol{P}}_k = \sum_{i=1}^{N} \tilde{\delta}_k^{(i)}\left(\boldsymbol{P}_k^{+(i)} + \left(\boldsymbol{x}_k^{+(i)} - \hat{\boldsymbol{x}}_k\right)\left(\boldsymbol{x}_k^{+(i)} - \hat{\boldsymbol{x}}_k\right)^T\right) \tag{23}$$

A cycle in the EH_∞PF is completed with this logic. In summary, Equations (13)–(23) represent the steps used to obtain the a posteriori moments k from the a priori information

$(k-1)$ at a given instant of time. However, some important information about the EH_∞PF is listed here:

i. The EH_∞PF proposed here uses N particles with different values analyzing a possible sample impoverishment, a common problem for PF under the same conditions [3,20]. The idea is to analyze the processing time and the accuracy of the method.
ii. The weighting matrices $\boldsymbol{Q}_k$, $\boldsymbol{R}_k$, and $\boldsymbol{S}_k$ in EH_∞PF are designed as definite positive symmetric matrices and do not necessarily need to be diagonal, but the weighting matrices $\tilde{\boldsymbol{Q}}_k$ and $\tilde{\boldsymbol{R}}_k$ in EKF need to be configured as diagonals [3].
iii. Using the same weighting matrices $\boldsymbol{Q}_k$ and $\boldsymbol{R}_k$, it is observed that EH_∞PF has more robust results compared to EKF. According to the theory, the EH$_\infty$PF assumes that the process noise and measurement are both unmodeled, $\boldsymbol{w}_k$ and $\boldsymbol{v}_k$, respectively, and the initial condition $\boldsymbol{x}_0$ will be chosen to maximize the cost function of the problem, i.e., considering the worst case scenario for the estimation process.
iv. For an H_∞ filter, the threshold value of performance bound γ controls the unfavorable conditions of the method. According to [4], in the error estimation of the method, when the restricted projected parameter γ is reduced, the robustness characteristic of the filter is found. When the parameter γ assumes large values tending to infinity, the H_∞ filter has similar results to the standard Kalman filter.

4. Application and Results

The CBERS is a project for the development of remote sensing satellites administratively coordinated by the Brazilian Space Agency (AEB) and the China National Space Administration (CNSA), involving the scientific execution coordinated by the Brazilian National Institute for Space Research (INPE) and the Chinese Academy of Space Technology (CAST), which implements a world-class remote sensing system used by Brazil in strategic applications such as monitoring water resources, mapping the territory of both countries, and controlling deforestation in the Legal Amazon. In a first stage, the CBERS program started with two satellites, CBERS-1 and 2. With an agreement between Brazil and China, in November 2002, three satellites of the same category were built and launched, CBERS-2B, 3, and 4. In May 2015, a protocol for the development and launch of the CBERS 04A [28] was signed, and, more recently, in April 2023, an agreement was signed with the Chinese government to deepen scientific cooperation and collaborate on the development of the new CBERS-6 satellite. This satellite will have a new technology called synthetic aperture radar (SAR), which will increase and improve the monitoring of the Brazilian territory and biomes.

4.1. Parameters

The CBERS-4 satellite used in this research, the fifth satellite of the CBERS program, was launched on 7 December 2014 in a heliosynchronous and frozen orbit (see Figure 1). This configuration can provide global coverage: with low resolution cameras every 5 days, with medium resolution cameras every 26 days, and with high resolution cameras every 52 days [29].

In this work, in order to estimate the gyros bias and attitude, simulated orbit and attitude data from CBERS-4 were used, making use of the PROPAT propagator implemented in MatLab software. The PROPAT functions perform coordinate transformations, time and ephemeris conversion, orbital propagation, attitude transformations in various parameterizations, and attitude propagation [11]. The initial orbit and attitude conditions can be found in detail in [20]. In this article, the scope of the problem is expanded using a robust estimation method. This is supported by a series of additional simulations, including method comparison.

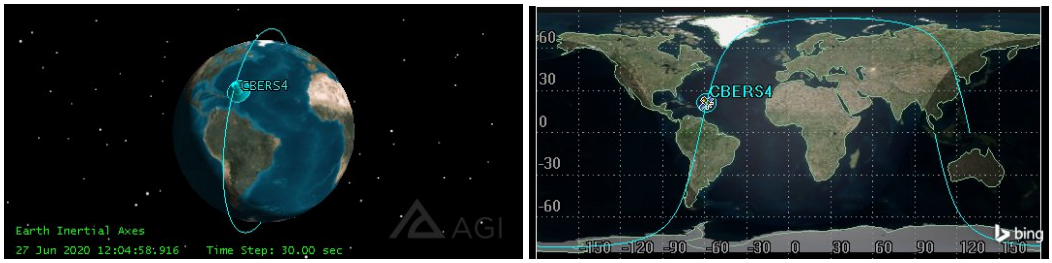

(**a**) (**b**)

Figure 1. Representative CBERS-4 orbit configuration, in (**a**) 3D orbit and (**b**) the respective groundtrack.

Table 1 presents CBERS-4 orbital parameters used for orbit simulation.

Table 1. CBERS-4 nominal orbital parameters [29].

Variable	Description	Values
a	Semi-major axis (average)	7148.865 km
e	Eccentricity	1.1×10^{-3}
i	Inclination	98.504 deg
Ω	Right ascension of the ascending node (RAAN)	333.3615 deg
ω	Perigee argument	117.4208 deg
t_{LTDN}	Local time at the descending node	10:30 a.m.
τ	Orbital period	100.26 min

Table 2 presents the simulation data for the sampling rate Δ; the observation time span T; the quaternions initial state $\boldsymbol{q}_0$ and the gyros bias initial state $\boldsymbol{\varepsilon}_0$ that compose the initial state vector $\boldsymbol{x}_0$; the quaternions variance $\boldsymbol{\sigma}^2_{P_q}$ and the gyros bias variance $\boldsymbol{\sigma}^2_{P_b}$ that compose the initial covariance matrix P_0; and γ, the user-specific performance bound for EH_∞PF exclusively.

Table 2. Temporal parameters, CBERS-4 initial state, and initial variance parameters for estimation methods.

Variable	Description	Values
Δ	Sampling rate	0.5 s
T	Observation time span	10 min
$\boldsymbol{q}_0^T$	Quaternions initial state	[0 0 0 1]
$\boldsymbol{\varepsilon}_0^T$	Gyros bias initial state	[5.7 4.8 2.6] deg/h
$\boldsymbol{\sigma}^2_{P_q}$	Quaternions variance	0.25 deg^2
$\boldsymbol{\sigma}^2_{P_b}$	Gyros bias variance	1.0 deg^2/h^2
γ	Specific performance bound	$\frac{1}{3}$

For CBERS-4, the telemetry data from the sensors arrives at the onboard computer in a fixed binary word length that translates into floating point values. The data sampling rates of the sensors are different and come asynchronously: 2 Hz for gyroscopes, 1 Hz for IRES-s, and 0.25 Hz for DSS-s. These telemetries recorded on board are downlinked and made available by the control center. We chose in the simulations to use a common sampling rate for all sensors; we chose gyros sampling rate of 2 Hz or 0.5 s, as shown in Table 2.

These data are used in all estimation methods of this work. It is important to say that the values of $\boldsymbol{\varepsilon}_0$ are typical drifts simulated for the CBERS-4 application. Thus, the initial state vector $\boldsymbol{x}_0$ and the initial covariance matrix $\boldsymbol{P}_0$ started in Table 2 are used in Equations (24) and (25) below:

$$\boldsymbol{x}_0 = \begin{bmatrix} \boldsymbol{q}_0^T & \boldsymbol{\varepsilon}_0^T \end{bmatrix}^T \tag{24}$$

$$\boldsymbol{P}_0 = diag\begin{pmatrix} \boldsymbol{\sigma}^2_{P_q} & \boldsymbol{\sigma}^2_{P_q} & \boldsymbol{\sigma}^2_{P_q} & \boldsymbol{\sigma}^2_{P_q} & \boldsymbol{\sigma}^2_{P_b} & \boldsymbol{\sigma}^2_{P_b} & \boldsymbol{\sigma}^2_{P_b} \end{pmatrix} \tag{25}$$

where $diag(.)$ means a diagonal matrix.

Table 3 presents the quaternions process noise variance $\boldsymbol{\sigma}^2_{Q_q}$, the gyros bias process noise variance $\boldsymbol{\sigma}^2_{Q_b}$, the DSS measurements noise variance $\boldsymbol{\sigma}^2_{R_{DSS}}$, and the IRES measurements process noise variance $\boldsymbol{\sigma}^2_{R_{IRES}}$. These variances compose the initial diagonal process noise covariance matrix $\boldsymbol{Q}_0$ and the initial diagonal measurements noise covariance matrix $\boldsymbol{R}_0$.

Table 3. CBERS-4 process noises variance parameters and measurements noises variance parameters for estimation methods.

Variable	Description	Values
$\boldsymbol{\sigma}^2_{Q_q}$	Quaternions process noises variance	0.1×10^{-3}
$\boldsymbol{\sigma}^2_{Q_b}$	Gyros bias process noises variance	0.1×10^{-5} deg^2/h^2
$\boldsymbol{\sigma}^2_{R_{DSS}}$	DSS measurements noises variance	0.36 deg^2
$\boldsymbol{\sigma}^2_{R_{IRES}}$	IRES measurements noises variance	0.36×10^{-2} deg^2/h^2

These initial process noise covariance matrix $\boldsymbol{Q}_0$ and the initial measurements noise covariance matrix $\boldsymbol{R}_0$ are presented in Equations (26) and (27) below.

$$\boldsymbol{Q}_0 = diag\begin{pmatrix} \boldsymbol{\sigma}^2_{Q_q} & \boldsymbol{\sigma}^2_{Q_q} & \boldsymbol{\sigma}^2_{Q_q} & \boldsymbol{\sigma}^2_{Q_q} & \boldsymbol{\sigma}^2_{Q_b} & \boldsymbol{\sigma}^2_{Q_b} & \boldsymbol{\sigma}^2_{Q_b} \end{pmatrix} \tag{26}$$

$$\boldsymbol{R}_0 = diag\begin{pmatrix} \boldsymbol{\sigma}^2_{R_{DSS}} & \boldsymbol{\sigma}^2_{R_{DSS}} & \boldsymbol{\sigma}^2_{R_{IRES}} & \boldsymbol{\sigma}^2_{R_{IRES}} \end{pmatrix} \tag{27}$$

These matrices are used in all estimation methods of this work, and for EH_∞PF, the matrices $\boldsymbol{L}_k = \boldsymbol{I}_{7\times7}$ and $\boldsymbol{S}_k = \boldsymbol{I}_{7\times7}$ throughout the simulation, to have the direct estimation of the state vector according to the theory.

4.2. Filter Performance

Two metrics were defined to evaluate filter performance.

4.2.1. Mean Error

The mean error is represented by Equation (28).

$$\bar{\boldsymbol{X}}_k = \frac{1}{N}\sum_{i=1}^{N} \tilde{\boldsymbol{X}}_k^{(i)} \tag{28}$$

where

$$\tilde{\boldsymbol{X}}_k^{(i)} = \hat{\boldsymbol{x}}_k^{(i)} - \boldsymbol{x}_k \tag{29}$$

Equation (29) represents the estimation error, the difference between the estimated state and the true state, and has been used to verify the accuracy of each filter's estimate.

The respective standard deviation of mean error is represented by:

$$\boldsymbol{\sigma}_{X_k} = \sqrt{\frac{1}{N-1}\sum_{i=1}^{N}\left(\tilde{\boldsymbol{X}}_k^{(i)} - \bar{\boldsymbol{X}}_k\right)^2} \tag{30}$$

4.2.2. Root Mean Squared Error

The root mean square error is represented by Equation (31).

$$\bar{\tilde{\mathbf{X}}}_k = \sqrt{\frac{1}{N}\sum_{i=1}^{N}\left(\tilde{\mathbf{X}}_k^{(i)}\right)^2} \tag{31}$$

These two metrics were calculated for each iteration over a large number M of Monte Carlo simulations. It was employed to obtain the mean error, the standard deviation, and the root mean squared error of the simulation.

4.3. Methodology

The standard PF was implemented using re-sampling in a systematic way to increase particle diversity [3,30] with the intention of evaluating and measuring the performance of the proposed EH_∞PF. More details about this estimation method and implementation can be found in [1,20,31]. The mean error, root mean square error (RMSE), and processing time cost of the estimation methods used were analyzed and compared.

In state estimation simulations, the standard PF used $N = 500$ and 1000 particles, and the EH_∞PF used $N = 10, 25, 50, 100, 200, 300$, and 500 particles (all with the specific performance bound $\gamma = \frac{1}{3}$). However, for the PF, only the results with 500 particles are presented, and for EH_∞PF, only the results with 100 particles are presented for the estimation error state. The results with different particles number were used in scenario comparison estimation error and for analyzing the processing time cost.

4.4. Results

The attitude and gyros bias estimation error are presented in Figure 2a–f. The results were obtained in quaternions and transformed into Euler angles (ZYX sequence using roll ϕ, pitch θ, and yaw ψ angles), for better interpretation.

Figure 2a–c present only the attitude estimation error for the following estimation methods: PF (500 particles) in blue, EH_∞PF (100 particles and $\gamma = \frac{1}{3}$) in red, and the results together with $\pm 3\sigma$ in yellow and magenta, representing a confidence interval considering the error as a normal probability distribution. In Figure 2d–f are present only the gyros bias estimation error following the same logic of representation and color code as in Figure 2a.

It is observed in Figure 2a–c that the EH_∞PF (100 particles) presents excellent and competitive precision for the attitude estimation error with a mean close to zero with a reduced number of particles compared to the PF, with their results within $\pm 3\sigma$ standard deviations. For PF (500 particles), the results for attitude errors in roll and yaw extrapolate the reference standard deviation, but the attitude error in pitch visually presents a satisfactory result within the standard deviation considered and with precision superior to EH_∞PF (100 particles and $\gamma = \frac{1}{3}$).

It is noted in Figure 2d–f that the EH_∞PF (100 particles and $\gamma = \frac{1}{3}$) presents good precision for the gyros bias estimation error with results within $\pm 3\sigma$ standard deviations. The PF (500 particles) present good results only for the y-axis gyros bias estimation error in the limit of the considered standard deviation; for the x-axis gyros bias estimation error and z-axis gyros bias estimation error, they present results that extrapolate the reference standard deviation.

Figure 2 shows that in the PF process, the estimation error does not decrease with the filter process and eventually converges toward a value outside $\pm 3\sigma$. This discrepancy is associated with the number of particles used. Most of the time, for the PF to obtain good results, it is necessary to use a high number of particles, as few particles generate a problem called sample impoverishment.

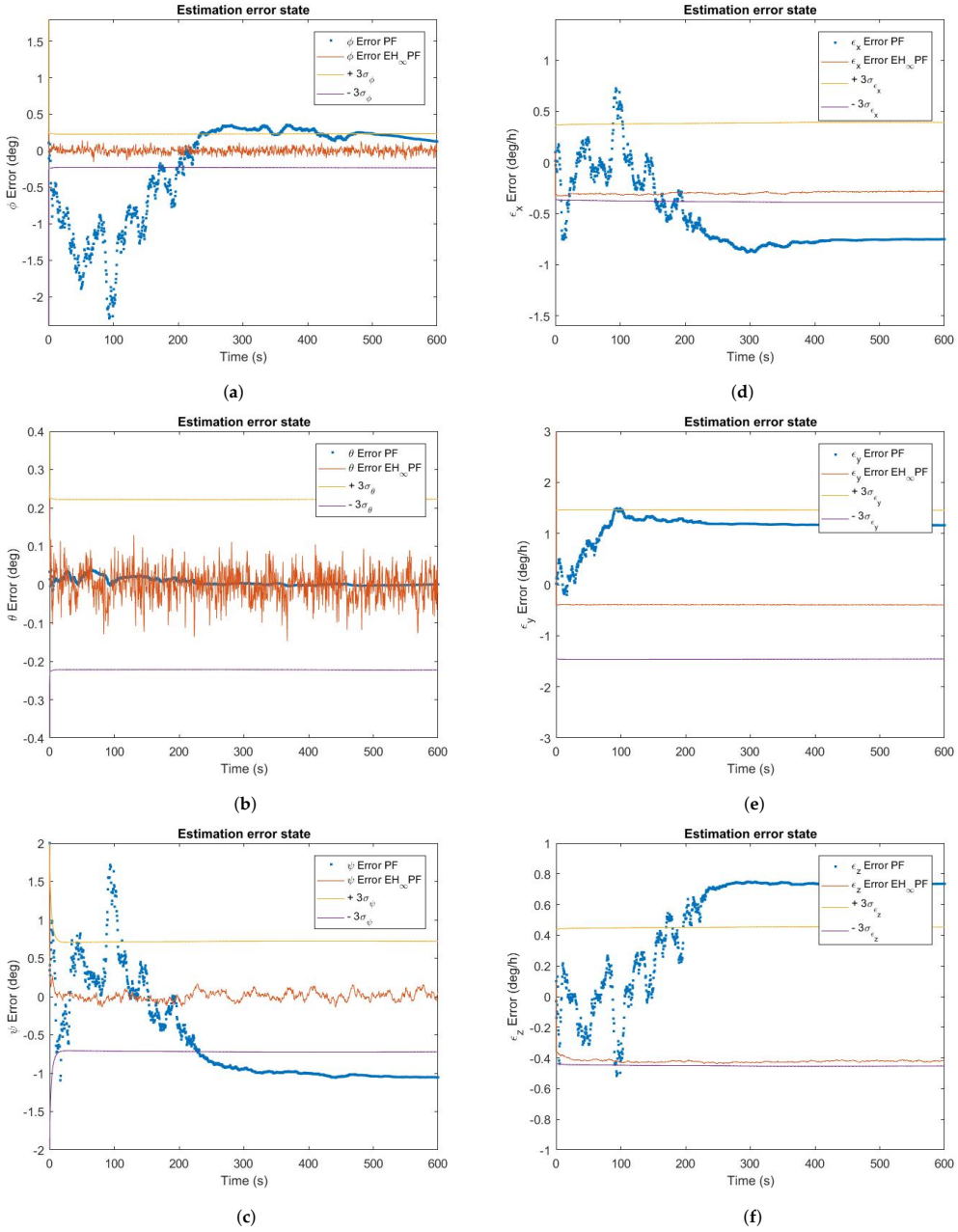

Figure 2. Graphical representation of the attitude and gyros bias estimation error using different estimation methods: PF (500 particles) and EH_∞PF (100 particles and $\gamma = \frac{1}{3}$). Results separated in the subfigures (**a**) roll estimation error, (**b**) pitch estimation error, (**c**) yaw estimation error, (**d**) x-axis gyros bias estimation error, (**e**) y-axis gyros bias estimation error and (**f**) z-axis gyros bias estimation error, for a simulation time of 10 min and a sampling rate of 0.5 s for the sensors.

Monolog graphs (Figure 3a–f) represent the scenarios that make up the estimation errors between the estimation methods used, facilitating the visualization with the following representation: PF (500 particles) in blue, EH_∞PF (100 particles) in red, EH_∞PF (50 particles) in yellow, and EH_∞PF (10 particles) in purple. All results for the EH_∞PF uses specific performance bound $\gamma = \frac{1}{3}$.

Figure 3a–c show that even with 100 particles, the EH_∞PF achieved a higher attitude determination accuracy in roll and yaw angle when compared to PF (500 particles). The standard PF did not achieve good accuracy even using a considerable number of particles, except for the pitch estimation error.

Comparing Figure 3d–f at the beginning of the simulation, the PF presents excellent results but it loses precision throughout the simulation. In this way, it is observed that the EH_∞PF with 100 particles reached a higher precision and accuracy for gyros bias estimation error when compared with standard PF.

In general, the EH_∞PF loses efficiency using a reduced number of particles, as can be seen in Figure 3a–f with 10 and 50 particles. For this attitude estimation application, the EH_∞PF with 100 particles showed, in terms of accuracy, competitive and interesting results.

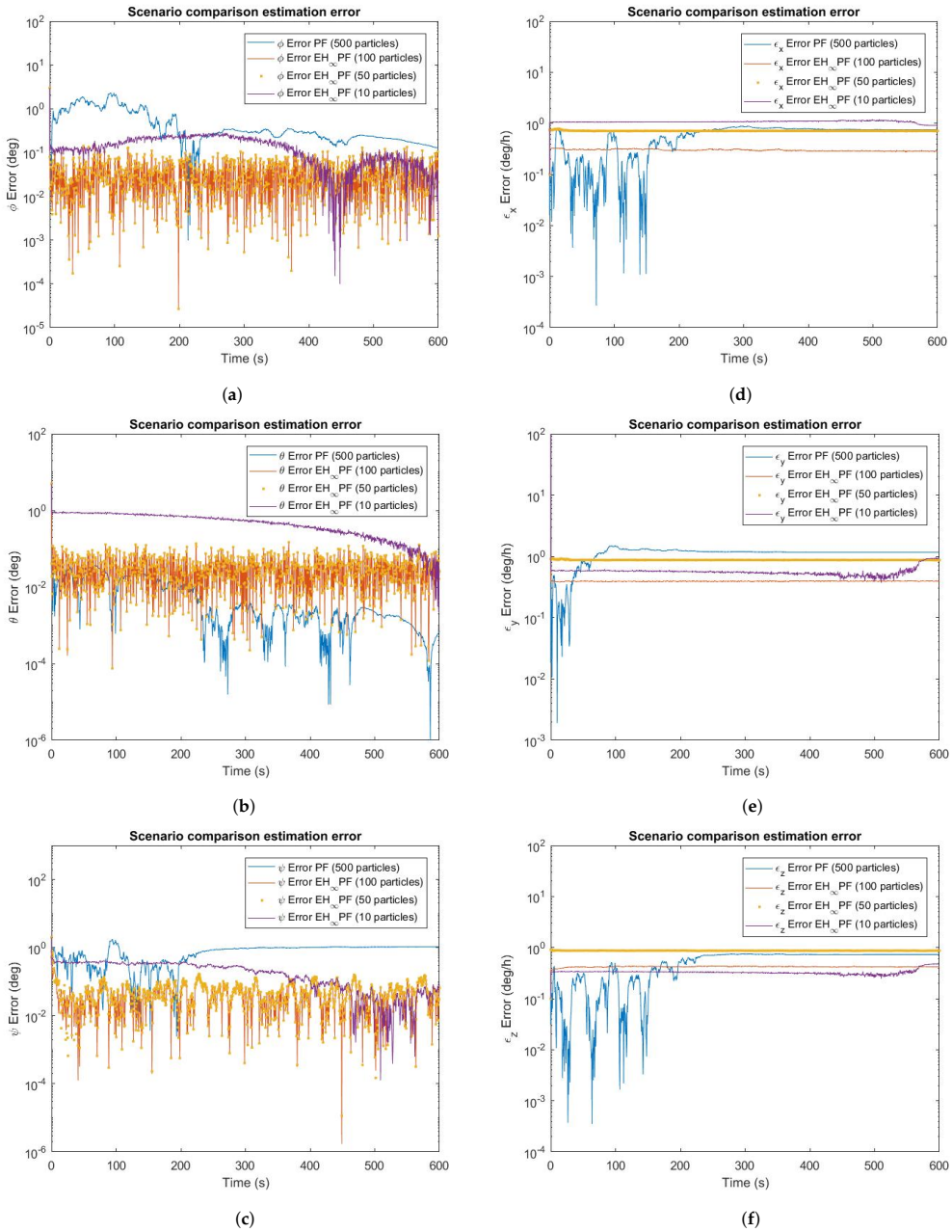

Figure 3. Monolog graphical representation of the attitude and gyros bias estimation error, comparison between different particles numbers for different estimation methods, PF and EH_∞PF ($\gamma = \frac{1}{3}$). Results separated in the subfigures (**a**) roll estimation error, (**b**) pitch estimation error, (**c**) yaw estimation error, (**d**) x-axis gyros bias estimation error, (**e**) y-axis gyros bias estimation error and (**f**) z-axis gyros bias estimation error, for a simulation time of 10 min and a sampling rate of 0.5 s for the sensors.

Tables 4 and 5 shows the mean error, standard deviation, minimal error, maximum error shown in Figure 2a–f, the RMSE, and peak to peak error in the attitude estimation and gyros bias estimation error for the PF (500 particles) and EH_∞PF (100 particles and $\gamma = \frac{1}{3}$).

Table 4. Summary statistical information presented on simulation range, mean error, standard deviation, minimum and maximum error, root mean square error, and peak-to-peak error for PF.

	PF					
	Mean Error	**Stand. Dev.**	**Min. Error**	**Max. Error**	**RMSE**	**Peak to Peak Error**
ϕ (deg)	−0.1938	0.6552	−2.2954	0.3544	0.3189	0.6299
θ (deg)	0.0063	0.0099	−0.0164	0.0390	0.0162	0.0424
ψ (deg)	−0.5745	0.6302	−1.0919	1.7162	1.8425	3.6840
ε_ϕ (deg/h)	−0.5500	0.3515	−0.8792	0.7237	2.1240	4.2480
ε_θ (deg/h)	1.1134	0.2754	−0.2004	1.4925	0.1472	2.2971
ε_ψ (deg/h)	0.5042	0.3404	−0.5174	0.7483	0.0982	1.1864

Table 5. Summary statistical information presented on simulation range, mean error, standard deviation, minimum and maximum error, root mean square error, and peak-to-peak error for EH_∞PF.

	EH_∞PF					
	Mean Error	**Stand. Dev.**	**Min. Error**	**Max. Error**	**RMSE**	**Peak to Peak Error**
ϕ (deg)	−0.0010	0.0416	−0.1474	0.1409	0.0010	0.320
θ (deg)	−0.0007	0.0410	−0.1475	0.2248	0.0009	0.4572
ψ (deg)	0.0085	0.0632	−0.1352	0.7358	0.0049	1.573
ε_ϕ (deg/h)	−0.2990	0.0118	−0.3307	−0.2769	0.0977	0.2894
ε_θ (deg/h)	−0.3926	0.0027	−0.4069	−0.3797	0.0824	0.1245
ε_ψ (deg/h)	−0.4216	0.0093	−0.4386	−0.3614	0.7515	1.4569

With the relation results of the estimation error, we found results of the order of 10^{-3} degrees on average (see Table 5) for the EH_∞PF considered within the design requirements for pointing error [29].

Table 6 presents the comparative information on data processing time for an Intel® Core™ i7 processor with a maximum frequency of 4.10 GHz for the estimation methods used. In summary, PF (500 particles) has a data processing time for state estimation 2.09 times greater than EH_∞PF (100 particles).

Table 6. Comparative information on data processing time.

Nonlinear State Estimation Method	**Processing Time (s)**
PF ($N = 500$ particles)	47.3310
PF ($N = 1000$ particles)	243.4860
EH_∞PF ($N = 10$ particles)	4.7782
EH_∞PF ($N = 25$ particles)	5.7672
EH_∞PF ($N = 50$ particles)	11.3551
EH_∞PF ($N = 100$ particles)	22.6254
EH_∞PF ($N = 200$ particles)	46.4539
EH_∞PF ($N = 300$ particles)	73.4110
EH_∞PF ($N = 500$ particles)	132.5640

5. Conclusions

The EH_∞PF based on the H_∞ filter is premised on minimizing the worst possible effects and conditions of disturbance signals associated with measurement noise through signal estimation error without a priori knowledge of these perturbations. The non-Gaussian uncertainties that appear in the process model are contained in the gyro's measurements, which present noise and bias due to post-launch sensor misalignment, thermal expansion, fading, electro-mechanical degradation, etc. All these factors cause inaccuracies in the model and deteriorate the attitude estimation process. The EH_∞PF proved to be effective for estimating attitude and showed greater accuracy when compared with the standard PF and results from previous studies using different estimation methods [1,16,17,20].

In summary, it is concluded that the EH_∞PF algorithm implemented in this work presented an excellent and competitive precision for estimating attitude and gyros bias;

the estimation error results are within a proposed confidence interval considering the error with a normalized Gaussian distribution. For EH_∞PF with coefficient of performance $\gamma = \frac{1}{3}$ and with only 100 particles, it presents a low data processing time, 2.09 times less than the standard PF with 500 particles. This represents an alternative to be used in embedded space systems. Both estimation methods converge without known sample impoverishment even using a reduced sample number, especially for EH_∞PF, with robust and fast results, providing a kinematic attitude solution in addition to estimating the gyroscope bias with specified accuracy for the attitude determination control system (ADCS) according to the project requirements.

Other results that could be presented would be evaluating the variation of performance threshold values γ as presented in [4] in order to verify the robustness of the EH_∞PF method, as already stated and theoretically validated. Reduced values of the performance coefficient γ would lead to the characteristic robustness of the filter. If the value of performance coefficient γ approaches infinity, the EH_∞PF would have results similar to the standard Kalman filter.

In future work, the research group intends to apply the attitude estimation method to other satellites such as the Amazônia I, from the National Institute for Space Research (INPE-Brasil); and in a cubesats scenario as for AlfaCrux [32] and SPLASH project—the Self-DePloyable FLexible AeroSHell for de-Orbiting and Space Re-entry [33]. Applications in other aerospace engineering dynamic systems will also be implemented, such as in-orbit estimation using GPS data and in aerodynamic coefficient estimation for unmanned aerial vehicles (UAV), for example. This application will analyze the precision, computational processing time cost, and feasibility to embedded systems.

Author Contributions: All authors contributed to the study conception and design. Conceptualization, W.R.S. and H.K.K.; methodology, W.R.S., R.V.G., P.C.P.M.P., and L.B.; software, W.R.S.; validation, W.R.S. and H.K.K.; formal analysis, investigation, and resources, W.R.S.; data curation, W.R.S. and H.K.K.; writing—original draft preparation, W.R.S.; writing—review and editing, W.R.S., M.C.F.P.S.Z., and H.K.K.; visualization, M.C.F.P.S.Z., R.V.G., P.C.P.M.P., and L.B.; supervision, H.K.K. and M.C.F.P.S.Z.; project administration and funding acquisition, W.R.S. and H.K.K. All authors have read and agreed to the published version of the manuscript.

Funding: National Council for Scientific and Technological Development (CNPq) grant number 307255/2018-2, 403801/2021-4.

Data Availability Statement: Data available on request due to privacy or ethical restrictions. The data presented in this study are available on request from the corresponding author. The data and codes are saved in non-public repositories, which can be provided upon request.

Acknowledgments: The authors are grateful for the financial support received by CNPq through project grant number 307255/2018-2, 403801/2021-4 and the Satellite Control Center of the Brazilian National Institute for Space Research (CCS-INPE) for the CBERS-4 data provided.

Conflicts of Interest: The authors declare no conflicts of interest. The authors declare that they have no known competing financial interests or personal relationships that could have appeared to influence the work reported in this paper.

References

1. Silva, W.R.; Garcia, R.V.; Kuga H.K.; Zanardi, M.C. Spacecraft Attitude Estimation using Unscented Kalman Filters, Regularized Particle Filter and Extended H_∞ Filter. *Adv. Astronaut. Sci.* **2017**, *162*, 1195–1214.
2. Iyer, R.; De, V.; Illikkal, R.; Koufaty, D.; Chitlur, B.; Herdrich, A.; Khellah, M.; Hamzaoglu, F.; Karl, E. Advances in Microprocessor Cache Architectures Over the Last 25 Years. *IEEE Micro* **2021**, *41*, 78–88. [CrossRef]
3. Simon, D. *Optimal State Estimation, Kalman, H_∞, and Nonlinear Approaches*; Wiley: New York, NY, USA, 2006.
4. Zhang, Q.; Meng, X.; Zhang, S.; Wang, Y. Singular value decomposition based robust cubature Kalman filtering for an integrated GPS/SINS navigation system. *J. Navig.* **2014**, *68*, 149–155. [CrossRef]
5. Banavar, R. A Game Theoretic Approach to Linear Dynamics Estimation. Ph.D. Thesis, University of Texas at Austin, Austin, TX, USA, 1992.
6. Shen, X. Discrete H_∞ filter design with application to speech enhancement. In Proceedings of the IEEE International Conference on Acoustics, Speech and Signal Processing, Detroit, MI, USA, 9–12 May 1995; pp. 1504–1507.

7. Shen, X.; Deng, L. Game theory approach to H_∞ discrete filter design. *IEEE Trans. Signal Process.* **1997**, *45*, 1092–1094. [CrossRef]
8. Hu, J.S.; Yang, C.H. Second-Order Extended H_∞ Filter for Nonlinear Discrete-Time Systems Using Quadratic Error Matrix Approximation. *IEEE Trans. Signal Process.* **2011**, *59*, 3110–3119. [CrossRef]
9. Einicke, G.A.; White, L.B. Robust Extended Kalman Filtering. *IEEE Trans. Signal Process.* **1999**, *47*, 2596–2599. [CrossRef]
10. Liu, J.; Cai, B.G.; Tang, T.; Wang, J. CKF-based robust filtering algorithm for GNSS/INS integrated train positioning. *J. Traffic Transp. Eng.* **2010**, *10*, 102–107.
11. Carrara, V. An Open Source Satellite Attitude and Orbit Simulator Toolbox for Matlab, International Symposium on Dynamic Problems of Mechanics, Natal, RN. 2015. Available online: http://mtc-m21b.sid.inpe.br/rep/sid.inpe.br/mtc-m21b/2015/04.07.13.24? (accessed on 16 February 2016).
12. Lefferts, E.J.; Markley, F.L.; Shuster, M.D. Kalman filtering for spacecraft attitude estimation. *J. Guid.* **1982**, *5*, 417–429. [CrossRef]
13. Crassidis, J.L.; Markley, F.L.; Cheng, Y. Survey of nonlinear attitude estimation methods. *J. Guid. Control. Dyn.* **2007**, *30*, 12–28. [CrossRef]
14. Shojaie, K.; Ahmadi, K.; Shahri, A.M. Effects of iteration in Kalman Filters family for improvement of estimation accuracy in simultaneous localization and mapping. In Proceedings of the IEEE/ASME International Conference on Advanced Intelligent Mechatronics, Zurich, Switzerland, 4–7 September 2007; pp. 1–6.
15. Garcia, R.V.; Kuga, H.K.; Zanardi, M.C. Using extended Kalman filter and least squares method for spacecraft attitude estimation. *Math. Eng. Sci. Aerosp.* **2011**, *2*, 445–453.
16. Garcia, R.V.; Kuga, H.K.; Zanardi, M.C. Unscented Kalman filter applied to the spacecraft attitude estimation with euler angles. *Math. Probl. Eng.* **2012**, *2012*, 985429. [CrossRef]
17. Garcia, R.V.; Kuga, H.K.; Zanardi, M.C. Unscented Kalman filter for spacecraft attitude estimation using quaternions and euler angles. In Proceedings of the International Symposium on Space Flight Dynamics, São José dos Campos, Brazil, 28 February–4 March 2011.
18. Pardal, P.C.P.M.; Kuga, H.K.; de Moraes, R.V. Analyzing the Unscented Kalman Filter Robustness for Orbit Determination through Global Positioning System Signals. *J. Aerosp. Technol. Manag.* **2013**, *5*, 395–408. [CrossRef]
19. Pardal, P.C.P.M.; de Moraes, R.V.; Kuga, H.K. Orbit Determination Using Nonlinear Particle Filter and GPS Measurements. In Proceedings of the AAS/AIAA Astrodynamics Specialist Conference, San Diego, CA, USA, 4–7 August 2014; pp. 1–6.
20. Silva, W.R.; Garcia, R.V.; Santilli, G.; Kuga, H.K.; Zanardi, M.C.F.P.S.; Pardal, P.C.P.M. Rao-Blackwellized Particle Filter for the CBERS-4 attitude and gyros bias estimation. *Acta Astronaut.* **2022**, *193*, 679–690. [CrossRef]
21. Shuster, M.D. A Survey of Attitude Representations. *J. Astronaut. Sci.* **1993**, *41*, 439–517.
22. Wertz, J.R. *Spacecraft Attitude Determination and Control*; D. Reidel: Dordrecht, The Netherlands, 1978.
23. Crassidis, J.L.; Junkins, J.L. *Optimal Estimation of Dynamic Systems*; Chapman and Hall/CRC Applied Mathematics and Nonlinear Science: New York, NY, USA, 2011.
24. Fuming, H.; Kuga, H.K. *CBERS Simulator Mathematical Models, CBTT Project, CBTT/2000/MM/001*; Instituto Nacional de Pesquisas Espaciais (INPE): São José dos Campos, Brazil, 1999.
25. Chen, Y.R.; Yuan, J.P. An improved robust H_∞ multiple fading fault-tolerant filtering algorithm for INS/GPS integrated navigation. *J. Astronaut.* **2009**, *30*, 930–936.
26. Rawicz, P.L. H_∞ / H_2 / Kalman Filtering of Linear Dynamics Systems via Variational Techniques with Applications to Target Tracking. Ph.D. Thesis, Drexel University, Philadelphia, PA, USA, 2000; p. 188.
27. Doucet, A.; de Freitas, N.; Gordon, N. *Sequential Monte Carlo Methods in Practice*; Springer: New York, NY, USA, 2001.
28. CBERS/INPE, Satélite Sino-Brasileiro de Recursos Terrestres-CBERS-INSTITUTO NACIONAL DE PESQUISAS ESPACIAIS, Available online: http://www.cbers.inpe.br/sobre/historia.php (accessed on 10 November 2022).
29. CBERS4/INPE, Satélite Sino-Brasileiro de Recursos Terrestres-CBERS-4-INSTITUTO NACIONAL DE PESQUISAS ESPACIAIS, Available online: http://www.cbers.inpe.br/sobre/orbita/cbers3-4.php (accessed on 20 June 2023).
30. Ristic, B.; Arulampalam, S.; Gordon, N. *Beyound the Kalman Filter, Particle Filters for Tracking Applications*; Artech House: Norwell, MA, USA, 2004.
31. Silva, W.R.; Kuga, H.K.; Zanardi, M.C. Application of the Regularized Particle Filter for Attitude Determination Using Real Measurements of CBERS-2 Satellite. *Adv. Astronaut. Sci.* **2015**, *15*, 1343–1360.
32. Borges, R.A.; dos Santos, A.C.; Silva, W.R.; Aguayo, L.; Borges, G.A.; Karam, M.M.; de Sousa, R.B.; García, B.F.-A.; Botelho, V.M.d.S.; Fernández-Carrillo, J.M.; et al. The AlfaCrux CubeSat Mission Description and Early Results. *Appl. Sci.* **2022**, *12*, 9764. [CrossRef]
33. Dimino, I.; Vendittozzi, C.; Reis Silva, W.; Ameduri, S.; Concilio, A. A Morphing Deployable Mechanism for Re-Entry Capsule Aeroshell. *Appl. Sci.* **2023**, *13*, 2783. [CrossRef]